Inorg. Chem. **2005**, *44*, 9752–9762

Pyridylporphyrin Metallacycles with a Slipped Cofacial Geometry: Spectroscopic, X-ray, and Photophysical Characterization

Elisabetta Iengo,*,† Ennio Zangrando,† Marco Bellini,† Enzo Alessio,*,† Anna Prodi,‡ Claudio Chiorboli,§ and Franco Scandola*,‡,§

Dipartimento di Scienze Chimiche, Università di Trieste, Via L. Giorgieri 1, 34127 Trieste, Italy, Dipartimento di Chimica, Università di Ferrara, 44100 Ferrara, Italy, and ISOF-CNR, Sezione di Ferrara, 44100 Ferrara, Italy

Received July 21, 2005

Treatment of the octahedral Ru(II) complex [*trans,cis,cis*-$RuCl_2(DMSO\text{-}O)_2(CO)_2$] with an equimolar amount of 5,10-bis(3′-pyridyl)-15,20-diphenylporphyrin (3′-*cis*-DPyP) yielded, upon selective replacement of the DMSO ligands, the neutral 2 + 2 metallacycle **2**. NMR spectroscopy provided unambiguous evidence that only one highly symmetrical species, in which the two chromophores are held in a slipped cofacial arrangement by the external Ru(II) metal fragments, exists in solution. The unprecedented geometry of **2**, and of the fully zincated analogue **2a**, were confirmed in the solid state by X-ray structural investigations. The spatial arrangement of the two parallel chromophores in **2**, with an interplanar distance of 4.18 Å and a lateral offset (center-to-center distance) of 9.82 Å, is reminiscent of those of the special pair of bacteriophylls in the reaction centers and of adjacent B850 units in the LH2 light-harvesting antenna systems of photosynthetic bacteria. For comparison, the X-ray structure of the corresponding metallacycle with 4′-*cis*-DPyP, **1a**, is also reported. In **1a**, the two porphyrins have an almost perfect coplanar arrangement. The semi-zincated metallacycles **1b** and **2b**, in which only one of the two chromophores bears an inner zinc atom, were prepared from **1** and **2**, respectively, and isolated in pure form. Detailed photophysical investigations of the above porphyrin assemblies were performed. In particular, very fast photoinduced intercomponent energy transfer processes from the zinc porphyrin to the free-base unit were detected in the semi-metalated derivatives **1b** and **2b** (time constants: 14 and 12 ps, respectively).

Introduction

Porphyrins and metallo−porphyrins play a relevant role in supramolecular chemistry, being frequently used as building blocks for the construction of artificial systems with special built-in properties or functions.[1] Among these, light-induced functions, particularly those inspired by natural photosynthesis, have attracted a great deal of attention.[2] Recently, the structures of the reaction centers of some purple- and cyano-bacteria have been determined by X-ray crystallography at very high resolution.[3] In all of these structures, the special pair, a dimer of bacteriochlorophylls that, upon excitation, initiates the first event of the charge-separation process, shows a very preservative spatial and geometrical arrangement: the two bacteriophylls are held in a parallel fashion with the planes at a distance ranging between 3 and 5 Å and with a lateral offset (center-to-center distance) in the range of 6.3−10 Å. In some cases, there is an edge-over-edge overlap involving one pyrrole group from each chromophore, with consequent partial overlap of

* To whom correspondence should be addressed. Phone: +390403955 (E.I.). Fax: +390403903 (E.I.). E-mail: iengo@dsch.units.it (E.I.), alessi@univ.trieste.it (E.A.), snf@unife.it (F.S.).

† Università di Trieste.

‡ Università di Ferrara.

§ Sezione di Ferrara.

(1) (a) *Comprehensive Supramolecular Chemistry*; Atwood, J. L., Davies, J. E., MacNicol, D. D., Vögtle, F., Eds.; Pergamon: Oxford, 1996; (b) Lehn, J.-M. *Supramolecular Chemistry: Concepts and Perspectives*; WCH: Wenheim, 1995.

(2) (a) Balzani, V.; Scandola, F. *Supramolecular Photochemistry*; Horwood: Chichester, U.K., 1991; (b) Balzani, V.; Scandola, F. In *Comprehensive Supramolecular Chemistry*; Atwood, J. L., Davies, J. E. D., MacNicol, D. D., Vögtle, F., Reinhoudt, D. N., Eds.; Pergamon: Oxford, 1996; Vol 10, pp 687−746.

(3) (a) Deisenhofer, J.; Epp, O.; Sinning, I.; Michel, H. *J. Mol. Biol.* **1995**, *246*, 429−457. (b) Allen, J. P.; Feher, G.; Yeates, T. O.; Komiya, H.; Rees, D. C. *Proc. Natl. Acad. Sci. U.S.A.* **1987**, *84*, 5730−5734. (c) Zouni, A.; Witt, H.-T.; Kern, J.; Fromme, P.; Krauss, N.; Saenger, W.; Orth, P. *Nature* **2001**, *409*, 739−743. (d) Ferreira, K. N.; Iverson, T. M.; Maghlaoui, K.; Barber, J.; Iwata, S. *Science* **2004**, *303*, 1831−1838. (e) Jordan, P.; Fromme, P.; Witt, H. T.; Klukas, O.; Saenger, W.; Krauss, N. *Nature* **2001**, *411*, 909−917.

10.1021/ic051210l CCC: $30.25
Published on Web 11/30/2005

π-orbitals. Although it is clear that such a rigid specific disposition of the two chromophores plays a role in the photosynthetic event, it is still uncertain whether, and to which extent, the electronic coupling between the two bacteriophylls is crucial for the occurrence of the charge-separation process.[4]

In attempting to mimick this photoinduced natural event, several types of covalently linked donor−acceptor systems, including complex architectures, have been prepared, and their photophysical properties have been investigated.[5] More simply, the special pair has inspired the design and preparation of cofacial bisporphyrin systems. These models consist of face-to-face dimers, made of two metalloporphyrins covalently bridged via rigid spacers.[6] To date, only a few groups have exploited the metal-mediated approach, which is usually much less synthetically demanding than the classical covalent one, for the construction of porphyrin-based models of the special pair.[7] In particular, Kobuke's models are based on self-coordinated zinc-imidazolylporphyrin dimers with a slipped cofacial geometry.[7d−f] In the dimers bearing pyromellitdiimide electron-acceptor substituents,[7f] photoinduced charge separation was found to be faster, and charge recombination slower, than in the corresponding monomers. Thus, the structural similarity with the special pair may also imply functional analogy.

Interest in porphyrin model systems with slipped cofacial geometries is not limited to mimicking the geometry of the special pair. In fact, high-resolution X-ray structures showed that a similar arrangement of chromophores is also present in the highly symmetrical chlorophyll rings of the light-harvesting antenna systems of photosynthetic bacteria.[8] The strong excitonic coupling between the chromophores is essential for the ultrafast energy propagation within such rings.

Chart 1

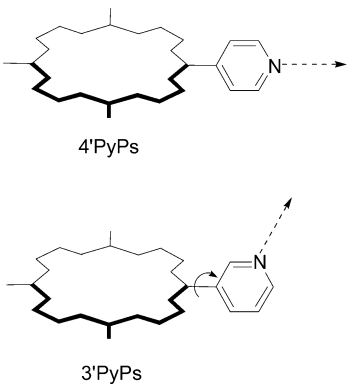

Particularly promising artificial metal-mediated porphyrin assemblies are those based on *meso*-4′-pyridyl/phenylporphyrins (4′PyPs). The coordinating ability of the peripheral 4′-pyridyl groups toward metal centers has been extensively exploited for assembling purposes, affording a great variety of metal−multiporphyrin discrete arrays, including metallacycles such as molecular squares.[9] On the other hand, there are relatively few examples of metal-mediated assemblies involving 3′-pyridylporphyrins (3′PyPs). The change in the position of the peripheral N atom(s) is expected to induce major changes in the architecture of the resulting systems. In fact, with 4′PyPs, the coordination bonds are established in the plane of the porphyrin, along the meso bond axis, whereas with 3′PyPs, the coordination bonds are directed out of the plane of the chromophore (Chart 1). Most of the work reported by us and by others concerned the use of 3′PyPs as units for the construction of *side-to-face* arrays via axial coordination to other metalloporphyrins.[10,11] Only two examples of discrete assemblies in which the 3′PyPs are connected via external coordination to metal centers have been reported.[12]

(4) (a) Won, Y.; Friesner, R. A. *Proc. Natl. Acad. Sci. U.S.A.* **1987**, *84*, 5511−5515. (b) Lathrop, E. J. P.; Friesner, R. A. *J. Phys. Chem.* **1994**, *98*, 3056−3066. (c) Laporte, L. L.; Palaniappan, V.; Kirmaier, C.; Davis, D. G.; Schenck, C. C.; Holten, D.; Bocian, D. F. *J. Phys. Chem.* **1996**, *100*, 17696−17707.

(5) (a) Wasielewski, M. R. *Chem. Rev.* **1992**, *92*, 435−461. (b) Harriman, A.; Sauvage, J.-P. *Chem. Soc. Rev.* **1996**, 41−48. (c) Gust, D.; Moore, T. A.; Moore, A. L. *Acc. Chem. Res.* **1993**, *26*, 198−205. (d) Bennett, I. M.; Vanegas Farfano, H. M.; Bogani, F.; Primak, A.; Liddell, P. A.; Otero, L.; Sereno, L.; Silber, J. J.; Moore, A. L.; Moore, T. A.; Gust, D. *Nature* **2002**, *420*, 398−401. (e) Smirnov, S. N.; Liddell, P. A.; Vlassiouk, I. V.; Teslja, A.; Kuciauskas, D.; Braun, C. L.; Moore, A. L.; Moore, T. A.; Gust, D. *J. Phys. Chem. A* **2003**, *107*, 7567−7573. (f) Guldi, D. M. *Pure Appl. Chem.* **2003**, *75*, 1069−1075. (g) Gould, S. L.; Kodis, G.; Palacios, R. E.; de la Garza, L.; Brune, A.; Gust, D.; Moore, T. A.; Moore, A. L. *J. Phys. Chem. B* **2004**, *108*, 10566−10580. (h) Rybtchinski, B.; Sinks, L. E.; Wasielewski, M. R. *J. Am. Chem. Soc.* **2004**, *126*, 12268−12269.

(6) (a) Fletcher, J. T.; Therien, M. J. *J. Am. Chem. Soc.* **2002**, *124*, 4298−4311. (b) Chang, C. J.; Loh, Z.-H.; Deng, Y.; Nocera, D. G. *Inorg. Chem.* **2003**, *42*, 8262−8269. (c) Yagi, S.; Masayuki, E.; Yonekura, I.; Takagishi, T.; Nakazumi, H. *J. Am. Chem. Soc.* **2003**, *125*, 4068−4069. (d) Faure, S.; Stern, C.; Espinosa, E.; Guilard, R.; Harvey, P. D. *Chem.−Eur. J.* **2005**, *11*, 3469−3481.

(7) (a) Stibrany, R. T.; Vasudeven, J.; Knapp, S.; Potenza, J. A.; Emge, T.; Schugar, H. J. *J. Am. Chem. Soc.* **1996**, *118*, 3980−3981. (b) Funatsu, K.; Imamura, T.; Ichimura, A.; Sasaki, Y. *Inorg. Chem.* **1998**, *37*, 4986−4995. (c) Fukushima, K.; Funatsu, K.; Ichimura, A.; Sasaki, Y.; Suzuki, M.; Fujihara, T.; Tsuge, K.; Imamura, T. *Inorg. Chem.* **2003**, *42*, 3187−3193. (d) Kobuke, Y.; Miyaji, H. *J. Am. Chem. Soc.* **1994**, *116*, 4111−4112. (e) Kobuke, Y.; Miyaji, H. *Bull. Chem. Soc. Jpn.* **1996**, *69*, 3563−3569. (f) Kobuke, Y.; Ogawa, K. *Bull. Chem. Soc. Jpn*. **2003**, *76*, 689−708. (g) Ozeki, H.; Nomoto, A.; Ogawa, K.; Kobuke, Y.; Murakami, M.; Hosoda, K.; Ohtani, M.; Nakashima, S.; Miyasaka, H.; Okada T. *Chem.−Eur. J.* **2004**, *10*, 6393−6401.

(8) (a) McDermott, G.; Prince, S. M.; Freer, A. A.; Hawthornthwaite-Lawless, A. M.; Papiz, M. Z.; Cogdell, R. J.; Isaacs, N. W. *Nature* **1995**, *374*, 517−523. (b) Kuhlbrandt, W. *Nature* **1995**, *374*, 497−498. (c) Papiz, M. Z.; Prince, S. M.; Howard, T.; Cogdell, R. J.; Isaacs, N. W. *J. Mol. Biol.* **2003**, *326*, 1523−1538.

(9) (a) Drain, C. M.; Lehn, J.-M. *J. Chem. Soc., Chem. Commun*. **1994**, 2313−2315. (b) Yuan, H.; Thomas, L.; Woo, L. K. *Inorg. Chem*. **1996**, *35*, 2808−2817. (c) Stang, P. J.; Fan, J.; Olenyuk, B. *Chem. Commun*. **1997**, 1453−1454. (d) Drain C. M.; Nifiatis, F.; Vasenko, A.; Batteas, J. D. *Angew. Chem., Int. Ed.* **1998**, *37*, 2344−2347. (e) Fan, J.; Whiteford, J. A.; Olenyuk, B.; Levin, M. D.; Stang, P. J.; Fleischer, E. B. *J. Am. Chem. Soc.* **1999**, *121*, 2741−2752. (f) Schmitz, M. M.; Leininger, S.; Fan, T.; Arif, A. M.; Stang, P. J. *Organometallics* **1999**, *18*, 4817−4824. (g) Iengo, E.; Milani, B.; Zangrando, E.; Geremia, S.; Alessio, E. *Angew. Chem., Int. Ed.* **2000**, *39*, 1096−1099. (h) Splan, K. E.; Keefe, M. H.; Massari, A. M.; Walters, K. A.; Hupp, J. T. *Inorg. Chem.* **2002**, *41*, 619−621 and refs therein.

(10) (a) Prodi, A.; Indelli, M. T.; Kleverlaan, C. J.; Scandola, F.; Alessio, E.; Gianferrara, T.; Marzilli, L. G. *Chem.−Eur. J.* **1999**, *5*, 2668−2679. (b) Alessio, E.; Geremia, S.; Mestroni, S.; Iengo, E.; Srnova, I.; Slouf, M. *Inorg. Chem*. **1999**, *38*, 869−875. (c) Alessio, E.; Geremia, S.; Mestroni, S.; Gianferrara, T.; Slouf, M.; Prodi, A. *Inorg. Chem*. **1999**, *38*, 2527−2529. (d) Alessio, E.; Ciani, E.; Iengo, E.; Kukushkin, V. Yu.; Marzilli, L. G. *Inorg. Chem.* **2000**, *39*, 1434−1443. (e) Prodi, A.; Indelli, M. T.; Kleverlaan, C. J.; Alessio, E.; Scandola, F. *Coord. Chem. Rev.* **2002**, *229*, 51−58;

Chart 2

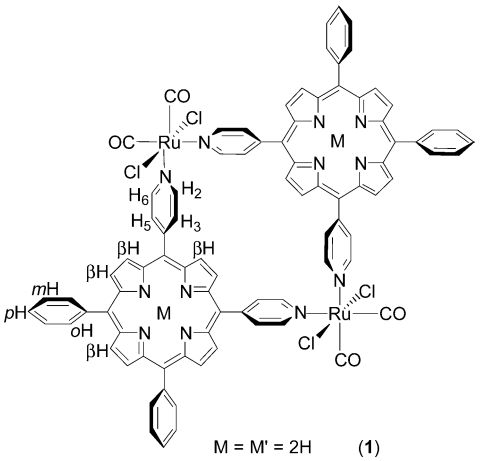

Recently, we described the neutral ruthenium-mediated 2 + 2 metallacycle **1** and its zinc derivative **1a**. **1** was prepared by treatment of the octahedral Ru(II) complex [*trans*,*cis*,*cis*-$RuCl_2(DMSO\text{-}O)_2(CO)_2$] with an equimolar amount of 5,10-bis(4′-pyridyl)-15,20-diphenylporphyrin (4′-*cis*-DPyP) (Chart 2).[13] We have now repeated this preparation using 3′-*cis*-DPyP instead of 4′-*cis*-DPyP and provide here unambiguous spectroscopic evidence that only one highly symmetrical 2 + 2 metallacycle, **2**, in which the two chromophores are held in a slipped cofacial arrangement by the external Ru(II) metal fragments, exists in solution. The unprecedented staggered geometry of **2** and of the fully zincated derivative **2a** (Chart 3) were confirmed in the solid state by X-ray structural investigations. For comparison, we also report the X-ray structure of **1a**, in which the two porphyrins have an almost perfect coplanar arrangement.

We also describe a detailed photophysical investigation of the above porphyrin metallacycles. In particular, efficient photoinduced intercomponent energy transfer processes from the zinc porphyrin to the free-base unit were observed for the semi-metalated dimers **1b** and **2b**.

Experimental Section

General Procedures. Hydrated $RuCl_3$ was a loan from Engehlard Italia. [*trans*,*cis*,*cis*-$RuCl_2(DMSO\text{-}O)_2(CO)_2$],[14] **1**,[13] and **1a**[13] were prepared as previously reported. 4′-*cis*-DPyP and 3′-*cis*-DPyP were synthesized and purified with the same procedure as that described by Fleischer and Shacter.[15] All reagents were analytical grade. Thin-layer chromatography was performed on silica plates (MERCK) using a 95/5 chloroform/ethanol mixture as eluent, unless differently stated. Column chromatography was performed on 40−63 μm mesh silica gel (BDH), unless otherwise specified. ^{1}H NMR and ^{13}C-{^{1}H} NMR spectra were recorded at 400 and 100.5 MHz, respectively, on a JEOL Eclipse 400 FT instrument or at 270 and 67.8 MHz, respectively, on a JEOL Eclipse 270 FT instrument. All spectra were run at room temperature in $CDCl_3$ (Aldrich), unless differently stated. Proton peak positions were referenced to the peak of residual nondeuterated chloroform set at 7.26 ppm. Carbon peak positions were referenced to the central peak of chloroform set at 77.0 ppm. Assignments were made with the aid of two-dimentional (2D) (H−H COSY and NOESY) and one-dimensional (1D) (difference-NOE) experiments. Solution ($CHCl_3$) infrared spectra were recorded in 0.1 mm cells with NaCl windows on a Perkin-Elmer 983G spectrometer.

UV−vis absorption spectra were recorded with a Perkin-Elmer Lambda 40 spectrophotometer. Nanosecond emission lifetimes were measured using a PRA system 3000 time-correlated single photon counting apparatus equipped with a Norland model 5000 MCA card and a hydrogen discharge pulsing lamp (50 kHz, halfwidth 2 ns). The decays were analyzed withEdinburgh FLA900 software. Nanosecond transient absorption spectra and lifetimes were measured with an Applied Photophysics laser flash photolysis apparatus, with frequency doubled (532 nm, 330 mJ) or tripled (355 nm, 160 mJ). Surelite Continuum II Nd:YAG laser (halfwidth 4−6 ns) Photomultiplier (Hamamatsu R928) signals were processed by a LeCroy 9360 (600 MHz, 5 Gs/s) digital oscilloscope. Femtosecond time-resolved experiments were performed using a pump−probe spectrometer based on the Spectra-Physics Hurricane Ti:sapphire system as a laser source and the Ultrafast Systems Helios spectrometer.[16] The pump pulse was generated either by a frequency doubler (400 nm) or with a Spectra Physics 800 OPA (tunable in the range of 320−700 nm). The probe pulse was obtained by continuum generation on a sapphire plate (useful spectral range, 450−800 nm). Effective time resolution ca. 300 fs, temporal chirp over the white-light 450−750 nm range ca. 200 fs, temporal window of the optical delay stage 0−1000 ps. The time-resolved spectral data were analyzed with the Ultrafast Systems Surface Explorer Pro software.

Data collections of **2** and **2a** were carried out at the X-ray diffraction beamline of the ELETTRA Synchrotron, Trieste (Italy), using the rotating crystal method with a monochromatic wavelength of 1.0000 Å on a MAR160-CCD detector. Measurements were performed at 100(2) K using a nitrogen stream cryo-cooler. The data set of **1a** was collected at 160(2) K on a Bruker-Nonius FR591 rotating anode (Cu Kα, λ = 1.54178 Å) equipped with a KappaCCD detector. Cell refinement, indexing, and scaling of the data sets were performed using the CCP4 package[17] and programs Denzo and Scalepack.[18] The structures were solved by direct methods and Fourier analyses and refined by the full-matrix least-squares method based on F^2 with all observed reflections.[19] ΔF maps revealed two disordered chloroform molecules for each dinuclear complex unit

(11) (a) Kariya, N.; Imamura, T.; Sasaki, Y. *Inorg. Chem.* **1998**, *37*, 1658−1660. (b) Funatsu, K.; Imamura, T.; Ichimura, A.; Sasaki, Y. *Inorg. Chem.* **1998**, *37*, 1798−1804. (c) Shinmori, H.; Kajiwara, T.; Osuka, A. *Tetrahedron Lett.* **2001**, *42*, 3617−3620. (d) Tsuda, A.; Sakamoto, S.; Yamaguchi, K.; Aida, T. *J. Am. Chem. Soc.* **2003**, *125*, 15722−15723. (e) Vinodu, M.; Goldberg, I. *Inorg. Chem.* **2004**, *43*, 7582−7584.

(12) (a) Sun, D.; Tham, F. S.; Reed, C. A.; Chaker, L.; Burgess, M.; Boyd, P. D. W. *J. Am. Chem. Soc.* **2000**, *122*, 10704−10705. (b) Sun, D.; Tham, F. S.; Reed, C. A.; Chaker, L.; Boyd, P. D. W. *J. Am. Chem. Soc.* **2002**, *124*, 6604−6612. (c) Fujita, N.; Birhadha, K.; Fujita, M.; Sakamoto, S.; Yamaguchi, K. *Angew. Chem., Int. Ed.* **2001**, *40*, 1718−1721.

(13) Iengo, E.; Zangrando, E.; Minatel, R.; Alessio, E. *J. Am. Chem. Soc.* **2002**, *124*, 1003−1013.

(14) Alessio, E.; Milani, B.; Bolle, M.; Mestroni, G.; Faleschini, P.; Todone, F.; Geremia, S.; Calligaris M. *Inorg. Chem.* **1995**, *34*, 4722−4734.

(15) Fleischer, E. B.; Shacter, A. M. *Inorg. Chem.* **1991**, *30*, 3763−3769.

(16) Chiorboli, C.; Rodgers, M. A. J.; Scandola. F. *J. Am. Chem. Soc.* **2003**, *125*, 483−491.

(17) Collaborative Computational Project, Number 4; *Acta Crystallogr., Sect. D: Biol. Crystallogr.* **1994**, *50*, 760−763.

(18) Otwinowski Z.; Minor, W. In *Processing of X-ray Diffraction Data Collected in Oscillation Mode*; Carter, C. W., Jr., Sweet, R. M., Eds.; Methods in Enzymology, Volume 276: Macromolecular Crystallography, Part A; Academic Press: New York, 1997; pp 307−326.

(19) Sheldrick, G. M. *SHELX97, Programs for Crystal Structure Analysis*, release 97-2; University of Göttingen: Germany, 1998.

Table 1. Crystallographic Data and Details of Refinements for **2**, **2a**, and **1a**

	2	**2a**	**1a**
solvent	$1.5C_6H_{14}$ $2CHCl_3$	$3CHCl_3$	$8CHCl_3$
formula	$C_{99}H_{79}Cl_{10}N_{12}O_4Ru_2$	$C_{95}H_{67}Cl_{13}N_{12}O_6Ru_2Zn_2$	$C_{100}H_{72}Cl_{28}N_{12}O_6Ru_2Zn_2$
M_r	2057.38	2256.26	2863.18
crystal system	monoclinic	triclinic	monoclinic
space group	$P2_1/c$	$P\bar{1}$	$P2_1/c$
temp (K)	100(2)	100(2)	160(2)
λ (Å)	1.00000	1.00000	1.54178
a (Å)	19.220(5)	15.873(4)	11.239(4)
b (Å)	17.341(5)	18.597(5)	14.018(4)
c (Å)	15.145(4)	19.372(5)	37.997(7)
α (deg)		65.88(2)	
β (deg)	107.72(3)	85.53(2)	90.95(3)
γ (deg)		78.18(2)	
volume (Å^3)	4808(2)	5108(2)	5986(3)
Z	2	2	2
D_{calcd} (g cm^{-3})	1.421	1.473	1.590
μ(Mo Kα) (mm^{-1})	1.966	2.817	8.662
F(000)	2094	2276	2860
θ range (deg)	3.54−29.28	2.36−31.60	3.36−60.12
reflns collected	18728	28979	25707
unique reflns	4351	10900	8554
R_{int}	0.0570	0.0790	0.0661
observed ($I > 2\sigma(I)$)	3994	7924	6445
parameters	546	1195	680
GOF (F^2)	1.086	1.176	1.056
R1 ($I > 2\sigma(I)$)	0.0938	0.0983	0.0761
wR2	0.2549	0.2713	0.2269
$\Delta\rho$ (e/Å^3)	1.016, −1.091	1.434, −0.852	1.075, −1.040

Chart 3

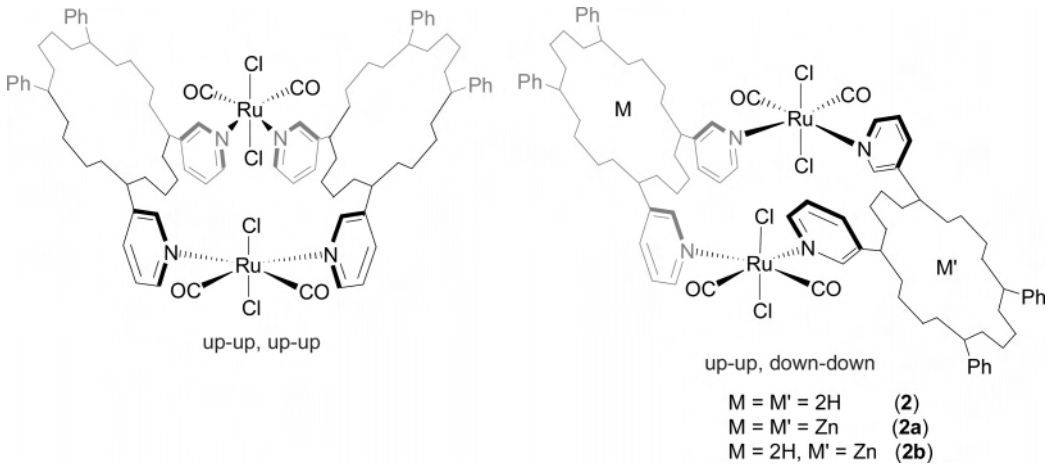

in **2**, three molecules in **2a**, and eight molecules in **1a**. Crystals of **2a** revealed also 1.5 molecules of *n*-hexane.

The solvent accessible void for the structures reported was evaluated to be 29.5 (**2a**), 27.9 (**2**), and 42% (**1a**) of the cell volume using the PLATON program.[20] Crystal data and details of structure refinements are reported in Table 1. All of the calculations were performed using the WinGX System, Ver. 1.64.05.[21]

Synthesis and Characterization. 1b. A 25-mg amount of **1** (0.015 mmol) dissolved in $CHCl_3$ (5 mL) was treated with 1.6 mg of $Zn(CH_3COO)_2 \cdot 2H_2O$ (0.0072 mmol) dissolved in the minimum amount of MeOH. After ca. 16 h, the solvent was removed in vacuo, and the residual purple powder was filtered after the addition of methanol. The solid was thoroughly washed with cold methanol and diethyl ether and vacuum-dried. Thin-layer chromatography of the crude product (alumina plates, eluent $CHCl_3$) showed it to contain **1b** ($R_f = 0.30$) together with **1** and **1a**. Pure **1b** was obtained as the second band from a column eluted with chloroform (stationary phase: aluminum oxide, activated neutral, Brockmann I (Aldrich)). Yield: 14 mg (55%). ^{1}H NMR spectrum ($CDCl_3$) (the protons labeled with Zn belong to the zincated porphyrin, see Chart 2 for labeling scheme): δ = 9.84 (d, 4H, $H_{2,6}$Zn); 9.81 (d, 4H, $H_{2,6}$); 9.16 (m, 6H, βHZn); 9.07 (m, 6H, βH); 9.04 (s, 2H, βHZn); 8.91 (s, 2H, βH); 8.60 (d, 4H, $H_{3,5}$Zn); 8.57 (d, 4H, $H_{3,5}$); 8.26 (m, 8H, *o*-H); 7.84 (m, 12H, *m*- + *p*-H); −2.71 (s, 2H, −NH). UV−vis spectrum (λ_{max} (nm), $\epsilon \times 10^{-4}$ (cm^{-1} M^{-1})) in CH_2Cl_2: 427 (40.7), 492 (sh 0.34), 519 (1.37), 556 (1.96), 594 (0.77), 649 (0.30).

2. A mixture of 3′-*cis*-DPyP (21.0 mg, 0.031 mmol) and [*trans*,-*cis*,*cis*-$RuCl_2(DMSO\text{-}O)_2(CO)_2$] (12.0 mg, 0.031 mmol) dissolved in $CHCl_3$ (10 mL) was allowed to react for 2 days at room temperature. Thin-layer chromatography of the crude product, after solvent removal in vacuo, showed it to contain **2** (R_f = 0.72) together with other minor species. Pure **2** was obtained as the first band from a column eluted with chloroform. Yield: 20 mg (76.3%).

(20) Spek, A. L. *Acta Crystallogr., Sect A: Found. Crystallogr.* **1990**, *46*, C34.
(21) Farrugia, L. J. *J. Appl. Crystallogr.* **1999**, *32*, 837−838.

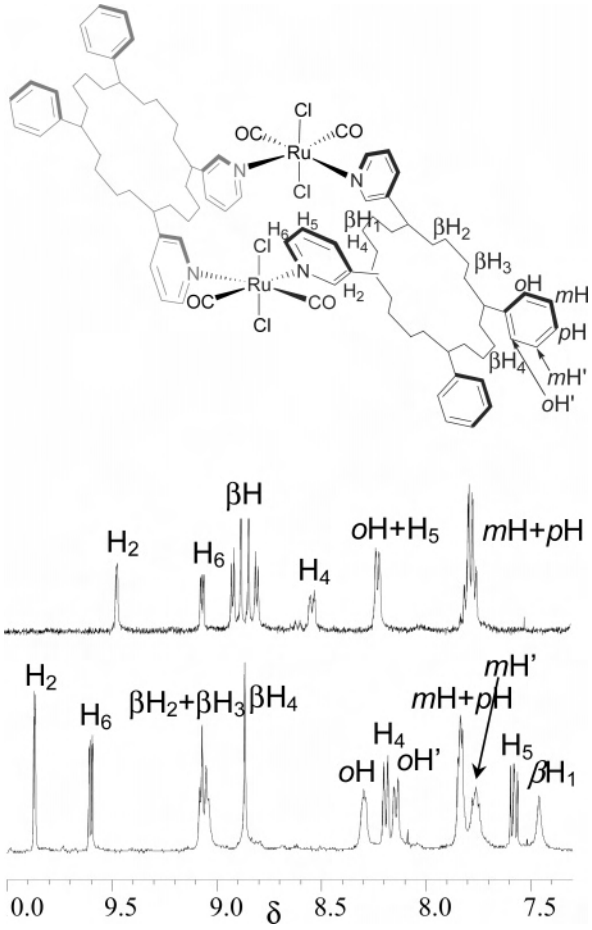

Figure 1. Schematic drawing of **2** with labeling scheme; aromatic region of its ^{1}H NMR spectrum ($CDCl_3$, below) as compared with the same spectral region of 3′-*cis*-DPyP (above).

^{1}H NMR spectrum ($CDCl_3$) (see Figure 1 for labeling scheme): δ = 9.87 (s, 4H, H_2); 9.60 (m, 4H, H_6); 9.06 (m, 8H, βH); 8.87 (s, 4H, βH); 8.30 (d, 4H, *o*-H); 8.19 (m, 4H, H_4); 8.17 (d, 4H, *o*-H′); 7.84 (m, 8H, *m*- + *p*-H); 7.77 (m, 4H, *m*-H′); 7.58 (m, 4H, H_5); 7.47 (s, 4H, βH); −2.99 (s, 4H, −NH). Selected ^{13}C NMR resonances ($CDCl_3$): δ = 194.9 (CO). UV−vis spectrum (λ_{max} (nm), $\epsilon \times 10^{-4}$ (cm^{-1} M^{-1})) in CH_2Cl_2: 418 (48.1), 425 (49.6), 517 (3.52), 552 (1.34), 590 (1.11), 646 (0.60). Selected IR bands ($CHCl_3$): 2071 and 2011 cm^{-1} (ν C=O).

2a. A 25-mg amount of **2** (0.015 mmol) dissolved in $CHCl_3$ (5 mL) was treated with an 8-fold molar excess of $Zn(CH_3COO)_2 \cdot 2H_2O$ (26 mg) dissolved in the minimum amount of MeOH. Samples of the reaction mixture were periodically withdrawn, diluted in CH_2Cl_2, and tested by visible spectroscopy. The spectra indicated that the zinc insertion was complete (after ca. 16 h) when the four Q-bands of **1** collapsed to two bands (550 and 588 nm); the split Soret band underwent minor shifts (from 418/425 nm to 418/427 nm), accompained by a decrease of intensity (ϵ_{max} = 30×10^4 cm^{-1} M^{-1} for **2** vs $\epsilon_{max} = 50 \times 10^4$ cm^{-1} M^{-1} for **2a**). These spectral changes are similar to those found upon metalation of free porphyrins.[15] The product (R_f = 0.45) was precipitated by the addition of *n*-hexane, removed by filtration, washed thoroughly with cold methanol and diethyl ether, and vacuum-dried. Yield: 20.2 mg (75%). ^{1}H NMR spectrum ($CDCl_3$): δ = 9.90 (m, 4H, H_2); 9.58 (m, 4H, H_6); 9.14 (m, 8H, βH); 8.98 (s, 4H, βH); 8.25 (d, 4H, *o*-H); 8.20 (m, 4H, H_4); 8.13 (d, 4H, *o*-H′); 7.81 (m, 8H, *m*- + *p*-H); 7.75 (m, 4H, *m*-H′); 7.67 (s, 4H, βH_1); 7.58 (m, 4H, H_5). UV−vis spectrum (λ_{max} (nm), $\epsilon \times 10^{-4}$ (cm^{-1} M^{-1})) in CH_2Cl_2: 418 (30.5), 427 (26.4), 550 (1.91), 588 (0.30).

2b. This product was synthesized and purified with a procedure similar to that reported for **1b**. Starting from a 25-mg amount of **2**, the isolated yield of **2b** was 52%.^{1}H NMR spectrum ($CDCl_3$): δ = 9.90 (m, 4H, H_2Zn); 9.87 (m, 4H, H_2); 9.60 (m, 4H, H_6); 9.58 (m, 4H, H_6Zn); 9.13 (m, 6H, βHZn); 9.06 (m, 6H, βH); 8.98 (s, 2H, βHZn); 8.86 (s, 2H, βH); 8.26 (m, 4H, *o*-H + *o*-HZn); 8.20 (m, 4H, H_4 + H_4Zn); 8.14 (m, 4H, *o*-H′ + *o*-H′Zn); 7.82 (m, 8H, *m*- + *p*-H); 7.75 (m, 4H, *m*-H′ + *m*-H′Zn); 7.58 (m, 8H, H_5 + H_5Zn); 7.62 (s, 4H, βH + βHZn); −2.99 (s, 2H, −NH). UV−vis spectrum (λ_{max} (nm), $\epsilon \times 10^{-4}$ (cm^{-1} M^{-1})) in CH_2Cl_2: 418 (29.7), 426 (28.8), 481 (0.11), 517 (1.13), 552 (1.48), 590 (0.053).

Results and Discussion

Solution Studies. The treatment of 3′-*cis*-DPyP with an equimolar amount of [*trans*,*cis*,*cis*-$RuCl_2$(DMSO-O)$_2$(CO)$_2$] led to the formation of a main product, **2** (Chart 3), that was easily obtained in pure form by column chromatography. With a similar procedure, using 4′-*cis*-DPyP instead of 3′-*cis*-DPyP, we had previously obtained the 2 + 2 metallacycle **1** (Chart 2).[13] The high mobility of **2** on silica gel, similar to that of **1**, was a clear indication of its discrete cyclic nature, which was unambiguously established by ^{1}H NMR spectroscopy.

The following NMR spectral features ($CDCl_3$) all agree in indicating that **2** is a highly symmetrical neutral cyclic dimer featuring two porphyrins connected by two [*trans*,-*cis*-$RuCl_2(CO)_2$] fragments (Figure 1): (i) there are no signals for residual DMSO coordinated to Ru, consistent with the complete substitution of these labile ligands by the pyridyl rings; (ii) the H_2 and the H_6 resonances of the 3′N(py) rings are downfield shifted compared to those of unbound 3′-*cis*-DPyP ($\Delta\delta$ = 0.37 and 0.54, respectively), as expected for coordination to ruthenium;[22] (iii) there is only one set of signals for the porphyrin protons; thus, the two chromophores are equivalent;[23] (iv) the resonances of the pyrrole protons (βH), two singlets and two doublets of equal intensity, are consistent with a cis geometry for each porphyrin ring; (v) there is a single carbon resonance at δ = 194.9 for the equivalent CO groups. In addition, in the IR spectrum of **2** in chloroform solution, two carbonyl stretching bands are detected at 2071 and 2011 cm^{-1}, as expected for a cis geometry of the two CO molecules on each ruthenium fragment.

Two highly symmetrical limiting geometries are possible for **2**, in which both 3′-pyridyl rings on each porphyrin have a syn orientation with respect to the mean plane of the chromophore (Chart 3). In one case (labeled up−up, up−up), the two Ru atoms are above both porphyrins, which are thus facing each other with a narrow dihedral angle; in the other case (up−up, down−down), the two Ru atoms are above one porphyrin and below the other, and the two

(22) (a) Alessio, E.; Iengo, E.; Marzilli, L. G. *Supramol. Chem.* **2002**, *14*, 103−120. (b) Iengo, E.; Zangrando, E.; Alessio, E. *Eur. J. Inorg. Chem.* **2003**, *13*, 2361−2367.

(23) The pairs of ortho and meta phenyl protons are not equivalent, and their resonances are split into a pair of multiplets each (assignments were made with a NOESY experiment, see Supporting Information).

porphyrins are parallel to each other with a slipped cofacial arrangement.

A careful exam of the NMR spectrum (Figure 1) allowed us to establish that, in solution, **2** assumes the slipped cofacial geometry (up−up, down−down) exclusively, consistent with what was found in the solid state by X-ray crystallography (see below). We observed that only one pyrrole singlet has an unusual upfield chemical shift ($\Delta\delta = -1.4$). This resonance was assigned to the two equivalent inner βH_1 protons by a difference-NOE experiment: its saturation induced a positive Overhauser effect on the signals of the nearby H_2 and H_4 protons of the cis pyridyl rings (see Supporting Information). The upfield shift localized on the βH_1 resonance was attributed to the mutual shielding of the two porphyrins, which affects them only marginally in this conformation. In the other conformer (up−up, up−up), the two porphyrin planes have a substantial overlap that would induce more generalized upfield shifts for all pyrrole resonances and for the −NH signal as well.

Variable temperature ^{1}H NMR experiments ($CDCl_3$), carried out in a range from −55 to +50 °C, induced no appreciable changes in the spectrum of **2**, indicating that, in the ΔT of observation, the adduct exists in solution as a single, stable conformer.

Another indication of the slipped cofacial disposition of the chromophores was the splitting of the Soret band (9 nm) observed in the visible absorption spectrum of **2**, suggesting the occurrence of an exciton interaction between the two porphyrins (see below), typical for this geometry.[7d]

Treatment of **2** with excess zinc acetate in chloroform/methanol mixtures led to the isolation of the corresponding zinc adduct **2a**. Except for the absence of the signal corresponding to the internal −NH protons, the ^{1}H NMR spectrum of **2a** ($CDCl_3$) is very similar to that described for the parent free-base metallacycle **2** (see Supporting Information). Therefore, **2a** has in solution the same staggered geometry as **2**.

Finally, treatment of **1** or **2** with only one equivalent of zinc acetate, followed by careful column chromatography, afforded in pure form the semi-zincated species **1b** and **2b**, respectively, in which only one of the two chromophores of each metallacycle has been metalated.[24] The ^{1}H NMR spectra of **1b** and **2b** are basically the sum of those of the corresponding free-base (**1** or **2**) and the fully zincated species (**1a** or **2a**); the −NH resonances integrate for two protons. Assignments were made accordingly. For each semi-zincated dimer, the resonances of the free-base and of the metalated porphyrin, with the exception of those of H_2 and H_6 in **1a**, overlap to some extent (see Experimental Section and Supporting Information).

1a and **2a** are particularly relevant for the photophysical investigations (see below), as the two chromophores on each metallacycle have different energy levels.

(24) **1b** has a mobility on silica gel that is intermediate between those of the corresponding free-base **1** and the fully zincated adduct **1a**. This guarantees that **1b** is a real species and not an equimolar mixture of **1** and **1a**. The same considerations apply to **2b**.

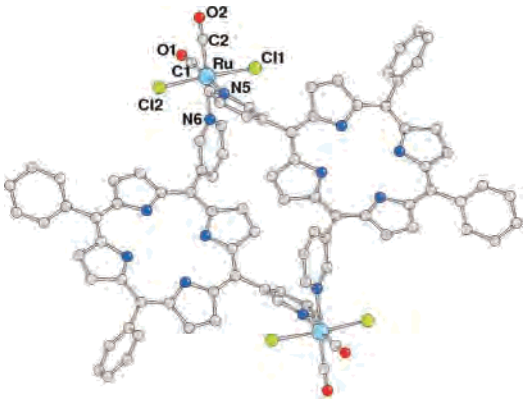

Figure 2. Molecular structure of **2** with atom-labeling scheme.

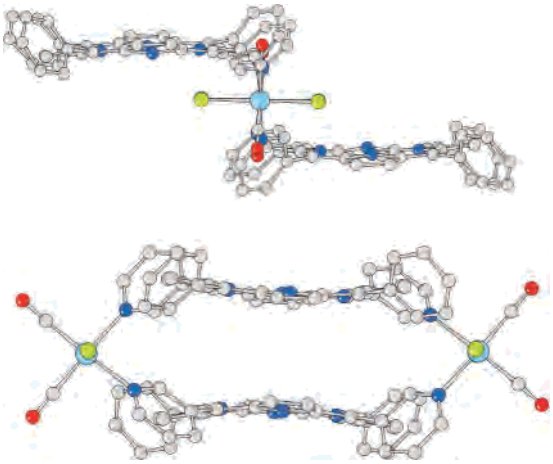

Figure 3. Two perspective side views of **2**: along the intermetallic vector that evidences the C_{2h} symmetry of the metallacycle (top), and along the Cl−Ru−Cl vector that evidences the porphyrin distortions (bottom).

Solid State. Single crystals of **2**, **2a**, and **1a**, suitable for X-ray investigation, were obtained by layering *n*-hexane on top of a $CHCl_3$ solution of each compound. The structural determination of **2** is consistent with the solution data: the two chromophores are held in a slipped cofacial arrangement by the external Ru(II) metal fragments (Figure 2). In the crystal, **2** is arranged around a center of symmetry and exhibits an ideal C_{2h} symmetry, with the two-fold axis passing through the Ru atoms (Figure 3). The two meso 3′-pyridyl rings on each porphyrin have a syn orientation and form dihedral angles of 45.5 and 61.7° with the mean plane of porphyrin to which they are attached. The ruthenium atoms are separated by 14.162(6) Å, and the distance between the porphyrin centroids is 9.819 Å (See Table 2). There is no overlap between the two macrocycles; the edge-to-edge distance, calculated between the C−C bonds of the inner pyrrole ring of each porphyrin, is about 1 Å. Each Ru atom presents a distorted octahedral environment with two trans chloride ligands and two pairs of cis carbonyls and pyridyl nitrogen atoms. The mean values of the Ru−C (1.84(1) Å), Ru−Cl (2.385(3) Å), and Ru−N (2.155(8) Å) bond distances are comparable to those found in analogous complexes.[22] The most significant deviation from the ideal geometry is the value of the N−Ru−N bond angle of 85.2(3)°.

A side view of the adduct along the parallel Cl−Ru−Cl axis shows the deformation of the macrocycles, which are

Table 2. Selected Bond Lengths (Å) of **2**, **2a**, and **1a**

		2a[a]		
	2[a]	molecule **A**	molecule **B**	**1a**
Ru−C(1)	1.877(12)	1.863(12)	1.839(11)	1.878(10)
Ru−C(2)	1.884(12)	1.834(14)	1.886(15)	1.870(8)
Ru−N(5)	2.171(8)	2.140(10)	2.148(10)	2.168(6)
Ru−N(6)	2.140(8)	2.157(10)	2.121(9)	2.161(6)
Ru−Cl(1)	2.393(3)	2.420(3)	2.394(3)	2.399(3)
Ru−Cl(2)	2.378(3)	2.381(3)	2.402(3)	2.386(2)
Zn−N(1)	−	2.070(8)	2.073(9)	2.062(6)
Zn−N(2)	−	2.030(10)	2.054(9)	2.085(6)
Zn−N(3)	−	2.065(8)	2.055(9)	2.061(6)
Zn−N(4)	−	2.053(9)	2.074(8)	2.057(6)
Zn−O(3)	−	2.133(8)	2.149(9)	2.162(6)
Ru−Ru′	14.162(6)	14.216(4)	14.110(4)	14.009(3)
Zn−Zn′	−	9.616(3)	10.421(4)	14.028(3)

[a] Labeling scheme for **2** and **2a** is the same as for **1a** (see Figure 5).

bowed toward each other (Figure 3). The vertical separation between the best-fit planes of the two porphyrins (interplanar distance) is 4.18 Å. The pyrrole carbon atoms are located alternatively above and below the 4N plane, with max deviations of ±0.49 Å. The meso phenyl rings form dihedral angles of 75.9 and 63.5° with the porphyrin mean plane.

The X-ray structural determination of the fully zincated metallacycle **2a** evidenced two independent molecules in the unit cell (**A** and **B**), both structurally very similar to **2**. The Ru atoms are ex-coordinated as expected (with bond distances comparable to those found in **2**), whereas each Zn ion presents a square pyramidal coordination geometry with four pyrrole N atoms in the basal plane and one ethanol molecule (from column chromatography) at the apical position. The Zn−N bond lengths fall in the range from 2.030(10) to 2.074(8) Å, whereas the Zn−O bonds are significantly longer (mean value 2.141(9) Å), with the metal displaced by 0.275(5) Å toward the axial ethanol oxygen donor. A view down the Ru−Ru vector evidences the configuration observed for the two independent molecules due to the different orientations assumed by the ethanol ligands: they are both oriented inward (with respect to the Ru atoms) in **A** and outward in **B** (Figure 4). The interporphyrin distance is 4.12 Å in **A** and 4.63 Å in **B**. The metal−metal distances in the two molecules are sensibly different: Ru···Ru in **A** (14.216(4) Å) is slightly longer than in **B** (14.110(4) Å), whereas the Zn···Zn distance is shorter in **A** (9.616(4) Å) than in **B** (10.421(4) Å).

The packing of both **2** and **2a** in the solid state is such to leave empty layers filled by solvent molecules (see Supporting Information).

The geometries of the slipped cofacial dimers bear a close similarity to some important structural motifs of natural photosynthesis: (a) the special pair of the photosynthetic reaction centers and (b) adjacent B850 chlorophyll molecules in the highly symmetrical rings of the LH2 light-harvesting antenna systems of bacterial photosynthesis.

The synthesis and spectroscopic characterization of the corresponding metallacycle with 4′-*cis*-DPyP, **1a**, had been previously reported by us,[13] but the X-ray structural determinations were performed on assemblies in which **1a** was axially bound through the Zn atoms to bridging heterocyclic

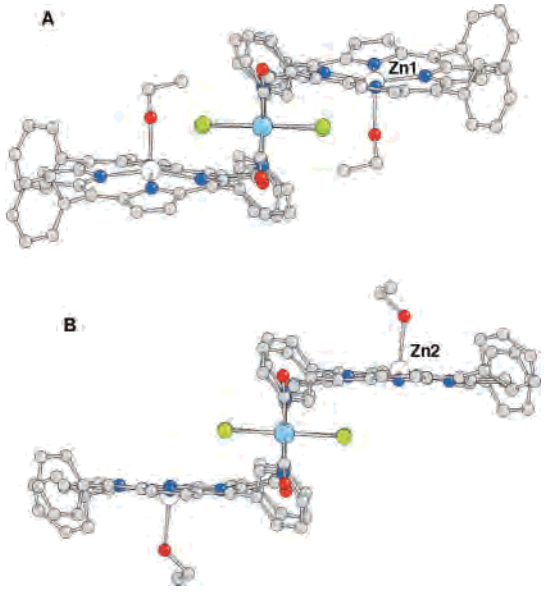

Figure 4. Side view along the Ru−Ru vector of the two crystallographic independent molecules **A** and **B** detected in the unit cell of **2a**. The deformations occurring in the macrocycles are clearly evident (max porphyrin atom deviations from the mean plane: +028/−0.38 Å in **A**, +0.29/−0.20 Å in **B**).

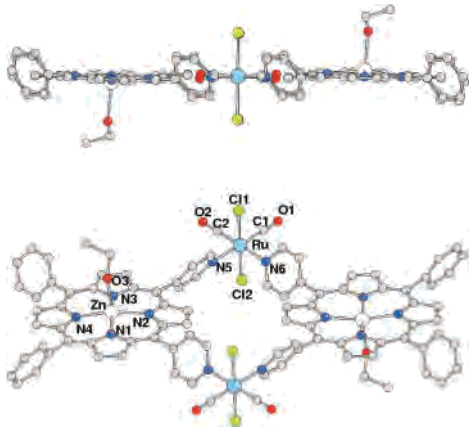

Figure 5. Perspective view of **1a** with atom-labeling scheme (bottom) and a side view along the Ru−Ru vector (top) showing the almost coplanar arrangement of the two porphyrin macrocycles.

N-ligands (4,4′-bipy or 4′-*trans*-DPyP), yielding either polymeric chains or discrete molecular sandwiches. We now describe the X-ray structure of **1a**, as we believe that a comparison with those of **2** and **2a** is revealing (Figure 5). **1a** has C_2 symmetry with the two-fold axis passing through the Ru atoms. The metallacycle is flat, with an almost perfect coplanar arrangement of the porphyrins (maximum deviations from the best-fit planes of −0.15 and +0.10 Å).

Interestingly, the other available X-ray structures of metal-mediated 2 + 2 metallacycles of porphyrins, with metal corners made by two $[Pd(dppp)]^{2+}$ (dppp = 1,2-bis(diphenylphosphino)propane) fragments[9f] or by one $[Pd(dppp)]^{2+}$ and one [*trans*,*cis*-$RuCl_2(CO)_2$] fragment,[9g] show that, in the solid state, these assemblies adopt a butterfly geometry, with dihedral angles between the two chromophores of 133 and 138°, respectively. Such orientations are very likely due to stacking interactions between the phenyl rings of dppp and the pyridyl rings of the porphyrins.

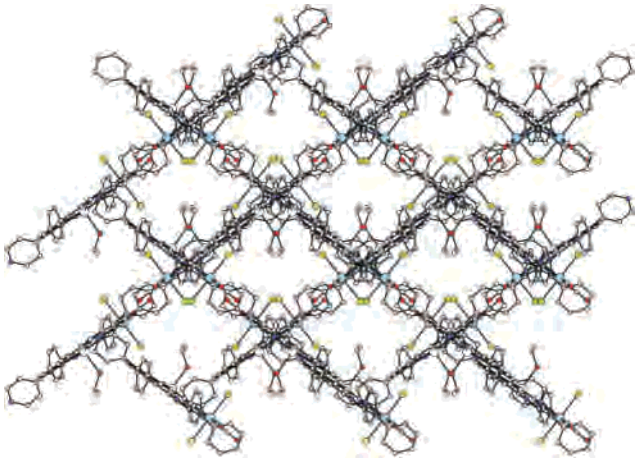

Figure 6. Packing of **1a**, view perpendicular to the *ab* plane (solvent molecules in the rhomboidal channels not reported for sake of clarity).

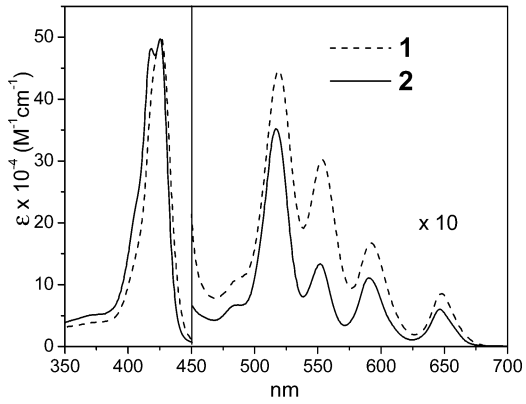

Figure 7. Absorption spectra of **1** and **2** in CH_2Cl_2.

In **1a**, the ruthenium octahedral ions have mean Ru−C (1.874(9) Å), Ru−Cl (2.393(2) Å), and Ru−N (2.164(6) Å) bond distances comparable to those found in **2** and **2a**. As in **2a**, each zinc ion of **1a** is axially bound to an ethanol molecule. The metals are practically located at vertexes of a square with Ru···Ru and Zn···Zn distances of 14.009(3) and 14.028(3) Å, respectively. In the crystal, the porphyrins are arranged normal to the crystallographic *ab* plane in such a way as to form rhomboidal channels, filled by solvent molecules, which account for 42% of the unit cell volume (Figure 6). This lattice void space is considerably larger than those calculated for the staggered structures **2a** and **2** (see Experimental Section). Indeed, there is a growing interest in neutral cyclic assemblies defining cavities and creating semi-infinite channel structures for microporous materials applications.[25] **1a** could act as building block to construct useful framework solids to be used, after solvent removal, for selective separation, chemical sensing, or catalysis.

Absorption Spectra. The absorption spectra of the corresponding pairs of flat and staggered metallacycles, **1** and **2**, **1a** and **2a**, and **1b** and **2b**, are compared in Figures 7, 8, and 9, respectively. As expected for weakly interacting systems, the spectra of **1**, **2** and **1a**, **2a** are very similar to

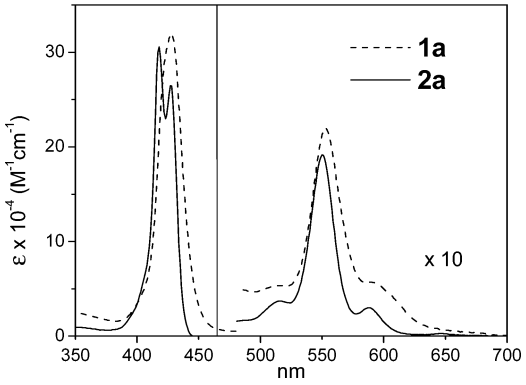

Figure 8. Absorption spectra of **1a** and **2a** in CH_2Cl_2.

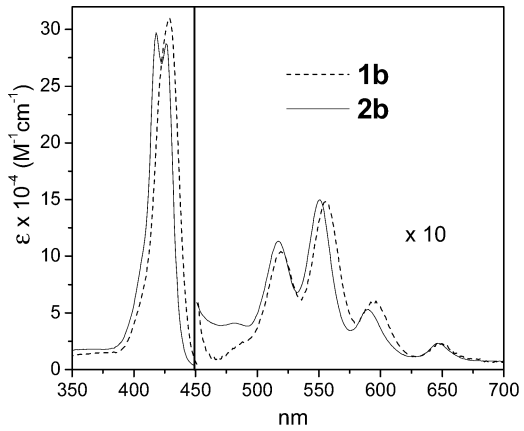

Figure 9. Absorption spectra of **1b** and **2b** in CH_2Cl_2.

those of the parent chromophores in the Q region, with the typical four-band and two-band[26] patterns for free-base and Zn-substituted porphyrins, respectively. A prominent difference between the planar and the slipped cofacial macrocycles is found in the Soret band region, in which a clear exciton splitting (of ca. 500 cm^{-1}) is present only for the latter compounds, **2** and **2a**. This difference can be easily rationalized. According to Kasha and co-workers,[27] in a point-dipole approximation, the exciton splitting for coplanar transition dipoles is given by

$$\Delta E = 2\,|\boldsymbol{M}|^2\,(1 - 3\cos^2\theta)\,r^{-3} \qquad (1)$$

where $\boldsymbol{M}$ is the transition moment of the monomer, r is the center-to-center distance, and θ is the angle between the transition dipoles. The center-to-center distance changes from 14.1 Å for the planar metallacycles to 10.1 Å for the staggered ones (see Solid State). On this basis, the exciton splitting for the planar geometry is expected to be about one-half of that for the staggered geometry, i.e., ca 250 cm^{-1}.[28] Given the actual bandwidth of 4′-*cis*-DPyP (ca 750 cm^{-1}), a single-maximum Soret band is expected for **1** and **1a**,**b**.

The spectra of the semi-zincated cyclic dimers **1b** and **2b** reflect with reasonable approximation the superposition of those of the porphyrin components. They show a five-band

(25) (a) Dinolfo, P. H.; Hupp, J. T. *Chem. Mater.* **2001**, *13*, 3113−3125. (b) Suslick, K. S.; Bhyrappa, P.; Chou, J.-H.; Kosal, M. E.; Nakagaky, S.; Smitherny, D. W.; Wilson, S. R. *Acc. Chem. Res.* **2005**, *38*, 283−291.

(26) The feature at 520 nm in the spectrum of **2a** is attributed to a minor (ca. 5%) amount of free-base absorption arising from incomplete Zn insertion.

(27) Kasha, M.; Rawls, H. R.; El-Bayoumi, M. A. *Pure Appl. Chem.* **1965**, *11*, 371−392.

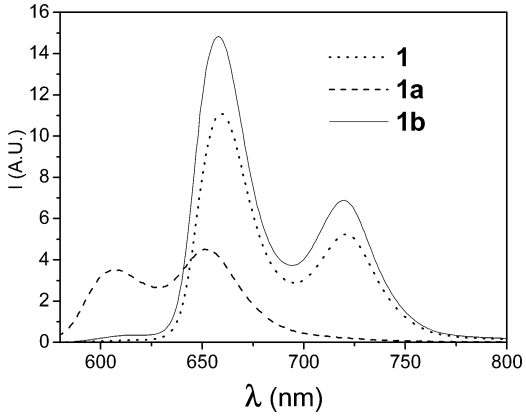

Figure 10. Emission spectra of **1**, **1a**, and **1b** in CH_2Cl_2.

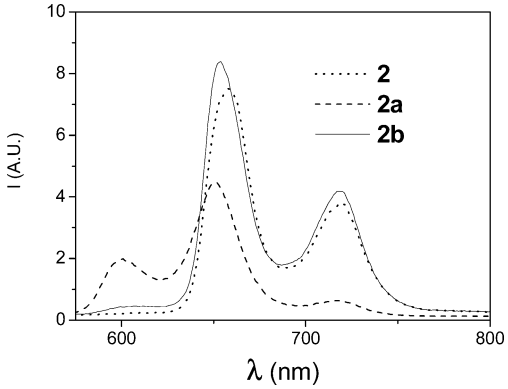

Figure 11. Emission spectra of **2**, **2a**, and **2b** in CH_2Cl_2.

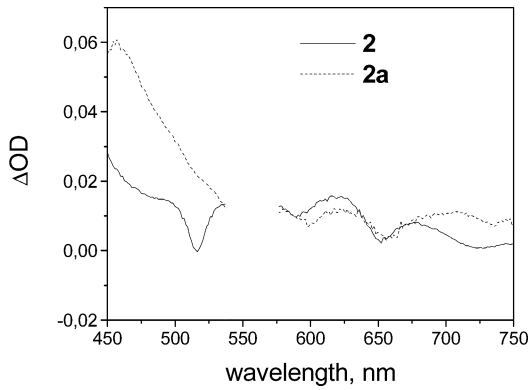

Figure 12. Transient spectra (constant over the 1−1000 ps time window) obtained for **2** and **2a** in $CHCl_3$. Time delay, 1 ps. Excitation wavelength, 555 nm.

pattern in the Q region (arising from the superposition of the four-band and two-band patterns of the free-base and Zn−porphyrin units, respectively). Again, the species **1b** shows a single Soret band, whereas **2b** exhibits exciton splitting. A comparison between the spectra of Figures 7, 8, and 9 shows that in the semi-zincated derivatives, selective excitation of the free-base porphyrin can be easily achieved using light of $\lambda > 600$ nm, whereas substantial (ca. 70%) excitation of the zincated porphyrin can be obtained with light of $\lambda = 550$ nm.

Photophysics. The emission measurements were carried out in dichloromethane solution. The laser photolysis experiments where carried out in chloroform solutions saturated with potassium carbonate to remove traces of acidity (that were found to promote photodecomposition under prolonged laser irradiation). Concentration-dependent spectrophotometric measurements demonstrated that in these conditions, the porphyrin metallacycles remain stable in highly diluted solutions ($\geq 1 \times 10^{-5}$ M). Freshly prepared solutions were always used. Photodecomposition was always negligible, as checked spectrophotometrically before and after each experiment.

Emission. The emission spectra of **1**, **1a**,**b**, **2**, and **2a**,**b** ($\lambda_{exc} = 550$ nm, comparable absorbance for all samples) are shown in Figures 10 and 11. Compounds **1**, **1a** and **2**, **2a** exhibit the typical fluorescence of the free-base or Zn−porphyrin units, respectively (**1**: $\lambda_{max} = 655$, 716 nm, $\tau = 5.7$ ns; **2**: $\lambda_{max} = 656$, 716 nm, $\tau = 5.5$ ns; **1a**: $\lambda_{max} = 608$, 651 nm, $\tau = 1.1$ ns; **2a**: $\lambda_{max} = 600$, 651 nm,[29] $\tau = 1.04$ ns). The lifetimes are somewhat shortened (by 30−40%) with respect to the porphyrin components as a consequence of the heavy-atom effect of the ruthenium centers.[30]

In the semi-zincated species **1b** and **2b**, despite the fact that the excitation wavelength is mainly absorbed by the Zn−porphyrin unit, only the free-base fluorescence is observed with appreciable intensity (**1b** $\lambda_{max} = 658$, 719 nm, $\tau = 5.0$ ns; **2b** $\lambda_{max} = 654$, 718 nm, $\tau = 5.3$ ns). This demonstrates the occurrence of efficient intramolecular singlet energy transfer from the Zn−porphyrin to the free-base unit. The efficiency of this process can be estimated by comparing the fluorescence intensity observed upon 550-nm excitation (ca. 70% Zn−porphyrin absorption) with that obtained upon 646-nm excitation (100% free-base absorption). After correction for the different absorbed light intensities (by comparison with optically matched solutions of a tetraphenylporphyrin standard), the emission intensities obtained for the two excitation wavelengths are identical within experimental error (ca. 5%). Thus, for both **1b** and **2b**, the efficiency of singlet energy transfer from the Zn−porphyrin to the free-base unit is ≥ 0.95.

Femtosecond Spectroscopy. The efficient quenching of the Zn−porphyrin emission implies that in the semi-zincated species **1b** and **2b**, intramolecular energy transfer takes place in the picosecond time scale. Therefore, ultrafast transient absorption experiments are required to monitor such processes. The experiments were performed using 555-nm excitation pulses to achieve substantial (ca. 70%) excitation of the Zn−porphyrin chromophore. The experiments performed on **2**, **2a**, and **2b** will be discussed in some detail.

The transient spectra obtained for **2** and **2a** are shown in Figure 12. For each compound, the bleaching of the ground-state Q-bands, superimposed on a broad, featureless excited-state absorption, is the fingerprint of the singlet excited state

(28) A detailed picture has to consider $\boldsymbol{M}_x$ and $\boldsymbol{M}_y$ transition dipoles for each porphyrin. With $\boldsymbol{M}_x$ oriented along the pseudo-C_2 axis of the *cis*-DPyP units, the following figures apply. **1**, **1a**,**b**: $\boldsymbol{M}_x$, $\theta = 0°$; $\boldsymbol{M}_y$, $\theta = 90°$. **2**, **2a**,**b**: $\boldsymbol{M}_x$, $\theta = 24°$; $\boldsymbol{M}_y$, $\theta = 90°$. With these figures, the expected exciton splittings (energy differences between the red-shifted *x*-polarized transition and the blue-shifted *y*-polarized transition) are calculated to be in a ratio 2.2 for staggered vs planar compounds (see Supporting Information).

(29) The feature at 720 nm is attributed to a minor (ca. 5%) amount of free-base emission arising from incomplete zinc insertion.

(30) Prodi, A.; Kleverlaan, C. J.; Indelli, M. T.; Scandola, F.; Alessio, E.; Iengo, E. *Inorg. Chem.* **2001**, *40*, 3498−3504.

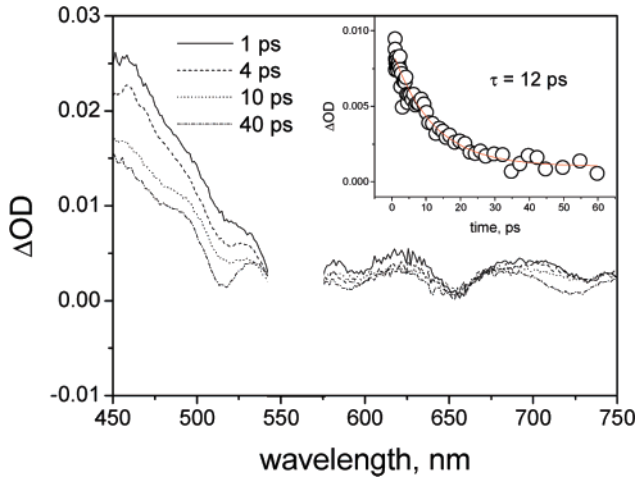

Figure 13. Transient spectral changes obtained for **2b** in $CHCl_3$. (Inset) Decay kinetics recorded at 515 nm. Excitation wavelength, 555 nm.

of the porphyrin units, either free-base (**2**) or zincated (**2a**). The transient spectra of the two metallacycles decay slowly in the ultrafast time scale, consistent with the lifetimes measured from fluorescence experiments (5.7 ns and 1.1 ns, respectively).

The spectral changes obtained for the semi-zincated dimer **2b** are shown in Figure 13. Consistent with the partitioning of the 555-nm light in favor of the Zn−porphyrin chromophore, the initial spectrum is similar to that of **2a** (Figure 12). Very rapidly, however, the transient spectrum undergoes substantial changes, with decreasing absorbance in the short-wavelength region and a characteristic bleaching developing at 515 nm. The final, constant spectrum reached after 40 ps very closely matches that of the free-base dimer **2**. These spectral changes provide clear, direct evidence for the occurrence of intramolecular singlet energy transfer in **2b** from the Zn−porphyrin to the free-base unit. The time constant of this process is 12 ps, corresponding to a rate constant $k = 8.3 \times 10^{10}$ s^{-1}. This value can be compared with that expected on the basis of the Förster theory of dipole−dipole energy transfer[31]

$$k = \frac{8.8 \times 10^{23} \kappa^2 \Phi_D}{n^4 R^6 \tau_D} \int F(\nu)\, \epsilon(\nu)\, \nu^{-4} d\nu \qquad (2)$$

where κ is a dipole−dipole orientation factor, Φ_D is the fluorescence quantum yield of the donor, n is the refractive index of the solvent, R is the center-to-center distance between donor and acceptor, τ_D is the fluorescence lifetime of the energy donor, $F(\nu)$ is the normalized fluorescence spectrum of the energy donor, and $\epsilon(\nu)$ is the absorption spectrum of the energy acceptor with molar extinction coefficient (M^{-1} cm^{-1}) unit. For the pair of zincated and free-base chromophores of **2b**, a center-to-center distance of 10.1 Å, a rate constant value of 4.8×10^{10} s^{-1} is predicted considering parallel transition moments.[32]

The results of the femtosecond experiments for the planar semi-zincated metallacycle **1b** are very similar to those described above for the slipped cofacial analogue **2b**. The transient spectral changes are almost identical to those shown in Figure 13, providing again clear evidence for singlet energy transfer from the Zn−porphyrin to the free-base unit. The kinetics, measured from the decay at 515 nm, give a time constant of 14 ps, again very similar to that obtained for **2b**. This result is somewhat surprising, as the longer center-to-center distance (14.1 Å in **1b** versus 10.1 Å in **2b**) would imply a smaller dipole−dipole interaction and a substantially slower Förster energy transfer (by a factor of ca. 7, considering parallel transition moments). In fact, the difference in dipole−dipole interactions between planar and staggered dimers is demonstrated by the different exciton splittings in their Soret bands (see above discussion and Figures 7, 8, and 9). Nevertheless, the energy transfer rate constants of **1b** and **2b** are comparable. A plausible explanation can be offered considering that singlet energy transfer in these systems may involve, in addition to through-space dipole−dipole interactions, some through-bond exchange interaction. This hypothesis has been proposed for several Zn−porphyrin/free-base dimeric systems showing rate constants larger than those predicted by eq 2.[33] In our ruthenium-bridged porphyrin metallacycles, through-bond interactions are expected to be more effective for 4′- than for 3′-pyridyl units (para rather than meta conjugation). Thus, in the planar macrocycle, a better exchange coupling could compensate for a weaker dipole−dipole interaction, leading to comparable energy transfer rate constants for the two systems.

A similar photoinduced energy transfer was observed by Hupp and co-workers in a 4′-*cis*-DPyP semi-zincated 2 + 2 metallacycle featuring $ReCl(CO)_3$ (rather than $RuCl_2(CO)_2$) corners.[9h] Rate constants of the order of 1×10^{10} s^{-1} were estimated from steady-state fluorescence measurements. The value measured here for **1b** by time-resolved absorption spectroscopy (7.1×10^{10} s^{-1}) is significantly higher. Given the different experimental methods used, it is difficult to tell whether this difference depends on the different nature of the metal corners in the systems.

Conclusions

We reported here the preparation and structural characterization of the 2 + 2 neutral porphyrin metallacycle **2**, which has, both in solution and in the solid state, a rigid slipped cofacial geometry of the two chromophores. The two porphyrins are held in this arrangement by the external Ru(II) metal fragments, with an interplanar distance of 4.18 Å and a lateral offset (centroid-to-centroid distance) of 9.82 Å. We

(31) (a) Förster, T. *Ann. Phys.* **1948**, *2*, 55−75. (b) Förster, T. *Discuss. Faraday Soc.* **1959**, *27*, 7−17.

(32) Appropriate values to be used in in eq 2 are: $n(CHCl_3) = 1.4459$; $\Phi_D/\tau_D = 1.8 \times 10^7$ s^{-1}; $\kappa^2 = (1 - 3\cos^2\theta)^2$, with $\theta = 90°$ for parallel transition dipoles. For aligned transition moments, $\theta = 24°$, and the calculated value is 1.9×10^{11} s^{-1}. Calculations performed using PhotochemCAD (Du, H.; Fuh, R. A.; Li, J.; Corkan, A.; Lindsey, J. S. *Photochem. Photobiol.* **1998**, *68*, 141−142).

(33) See, for example: (a) Gust, D.; Moore, T. A.; Moore, A. L.; Gao, F.; Luttrull, D.; DeGraziano, J. M.; Ma, X. C.; Makings, L. R.; Lee, S.-J.; Trier, T. T.; Bittersmann, E.; Seely, G. R.; Woodward, S.; Bensasson, R. V.; Rougee, M.; De Schryver F. C.; Van der Auweraer, M. *J. Am. Chem. Soc.* **1991**, *113*, 3638−3649. (b) Cho, H. S.; Kim, Y. H.; Kim, Y. R.; Jeoung, S. C.; Kim, D.; Kim, S. K.; Aratani, N.; Shinmori, H.; Osuka, A. *J. Phys. Chem. A* **2001**, *105*, 4200−4210.

had no evidence of the formation of other possible conformers of **2**, which might derive from variations in the orientations of the 3′N(py) rings. A very similar geometry was found for the fully zincated derivative **2a**. The geometry of **2** is unprecedented. By comparison, the corresponding metallacycle assembled with 4′-*cis*-DPyP as an angular fragment, **1a**, is almost perfectly flat. Therefore, the simple change in position of the peripheral pyridyl nitrogen atoms from 4′ to 3′ in the cis bifunctional donor ligand (4′-*cis*-DPyP vs 3′-*cis*-DPyP) results (after coordination to the same cis bifunctional ruthenium fragment [*trans,cis*-$RuCl_2(CO)_2$]) in dramatic structural differences in the final assemblies: from a flat 2D assembly in **1** to a staggered 3D structure with a rigid spatial arrangement of the two chromophores in **2**. Such an arrangement very closely resembles those found for the bacteriophylls of the special pair and of the antenna system (B850) of photosynthetic bacteria.

In a perspective of metal-mediated assembly of higher order, the zincated derivative **2a**, obtained by a remarkably simple synthetic procedure, is a new addition in the toolbox of building blocks for hierarchical constructions: if **1a** is a flat panel with two connecting points, **2a** is the corresponding steplike panel.

From a photophysical point of view, the symmetric dimers **2** and **2a** do not exhibit peculiar properties related to their slipped cofacial geometry, with emission energies and lifetimes similar to those of the planar analogues **1** and **1a**. Spectroscopically, however, a notable difference is observed in the Soret band region of their visible absorption spectra, in which a clear exciton splitting (of ca. 500 cm^{-1}) is present only for the staggered compounds, **2** and **2a**.

The semi-zincated metallacycles **1b** and **2b**, in which only one of the two chromophores bears an inner zinc atom, were prepared from **1** and **2**, respectively, and isolated in pure form.

In these species, 100%-efficient intramolecular singlet energy transfer was observed to occur from the Zn−poporphyrin to the free-base unit. The kinetics was studied by ultrafast spectroscopy following selective excitation of the zinc−porphyrin chromophore. The energy transfer processes were found to be very fast (14 and 12 ps for **1b** and **2b**, respectively). The similarity in rate constants probably reflects a substantial compensation between a stronger dipole−dipole interaction in the staggered system **2b** and a stronger through-bond interaction in the planar system **1b**.

Finally, the X-ray structure of **1b** evidenced the presence of rhomboidal channels, filled by solvent molecules, in the crystal lattice. This finding suggests that this flat, neutral metallacycle might be further investigated for microporous materials applications (e.g., chemical sensing).

Acknowledgments are made for financial support to the donors of the Petroleum Research Fund, administered by the ACS, (Grant ACS PRF# 38892-AC3) and to MIUR (PRIN 2003 no. 2003035553 and FIRB-RBNE019H9K projects). We thank Engelhard Italiana S.p.A. for a generous loan of hydrated $RuCl_3$. The CNR staff at ELETTRA (Trieste) are acknowledged for help in the use of the facility supported by CNR and by Elettra Scientific Division.

Supporting Information Available: 2D NOESY spectrum of **2** (aromatic region); diffNOE spectrum of **2** (aromatic region, irradiation on βH_1); ^1H NMR spectra of **2a** and **b** (aromatic region); crystal packing of **2**; calculation of exciton splittings for planar (**1a**,**b**) versus slipped cofacial metallacycles (**2**, **2a**, **2b**); tables of X-ray crystallographic data in CIF format for the structures reported in this paper. This material is available free of charge via the Internet at http://pubs.acs.org.

IC051210L